ENVIRONMENTAL RESEARCH
LETTERS

LETTER • OPEN ACCESS

Antarctic meltwater-induced dynamical changes in phytoplankton in the Southern Ocean

To cite this article: Ji-Hoon Oh *et al* 2022 *Environ. Res. Lett.* **17** 024022

IOP Publishing Environ. Res. Lett. 17 (2022) 024022 https://doi.org/10.1088/1748-9326/ac444e

ENVIRONMENTAL RESEARCH
LETTERS

OPEN ACCESS

RECEIVED
28 August 2021

REVISED
13 December 2021

ACCEPTED FOR PUBLICATION
17 December 2021

PUBLISHED
10 February 2022

LETTER

Antarctic meltwater-induced dynamical changes in phytoplankton in the Southern Ocean

Ji-Hoon Oh[1], Kyung Min Noh[1], Hyung-Gyu Lim[1,2], Emilia Kyung Jin[3], Sang-Yoon Jun[3] and Jong-Seong Kug[1,4,*]

[1] Division of Environmental Science and Engineering, Pohang University of Science and Technology (POSTECH), Pohang 37673, Republic of Korea
[2] Princeton University/Atmosphere and Oceanic Sciences Program, Princeton, NJ 08540, United States of America
[3] Korea Polar Research Institute (KOPRI), Incheon 21990, Republic of Korea
[4] Institute for Convergence Research and Education in Advanced Technology, Yonsei University, Seoul, Republic of Korea
[*] Author to whom any correspondence should be addressed.

E-mail: jskug@postech.ac.kr

Keywords: Antarctic meltwater, Antarctic ice-sheet/shelf, Southern Ocean, chlorophyll, phytoplankton

Supplementary material for this article is available online

Abstract

It has been suggested that the freshwater flux due to the recent melting of the Antarctic ice-sheet/shelf will suppress ventilation in the Southern Ocean (SO). In this study, we performed idealized earth-system simulations to examine the impacts of Antarctic meltwater on the biomass of surface phytoplankton in the Antarctic Ocean. The enhanced stratification due to the meltwater leads to a decrease in surface nitrate concentration, but an increase in the surface concentration of dissolved iron. These changes are associated with the reduced upwelling of nitrate-rich deep water and the trapped iron exported from terrestrial sediment. Because of the limited iron availability in the SO, the trapped iron in surface water enhances the chlorophyll concentration in the open ocean. However, in the marginal sea along the Antarctic coastline where the iron is relatively sufficient, a nitrate reduction induces a chlorophyll decrease, indicating a regime shift from iron-limited to nitrate-limited conditions.

1. Introduction

Recent observations have shown that the Antarctic ice-sheet/shelf is losing mass, resulting in a freshwater discharge into the Southern Ocean (SO) (Paolo *et al* 2015, Wouters *et al* 2015, Konrad *et al* 2018, Shepherd *et al* 2018, Rignot *et al* 2019). Under persistent greenhouse warming, freshwater released from from Antarctica may accelerate further (Fogwill *et al* 2015, DeConto and Pollard 2016, Hansen *et al* 2016). However, the effects of Antarctic meltwater have not been included in future projections in the Coupled Model Intercomparison Project Phase 5 (CMIP5) and the standard suite of CMIP6 (Taylor *et al* 2012, Eyring *et al* 2016). The ice-sheet had been mistakenly considered as a passive element of the climate system on sub-millennial timescales, but recent rapid melting of the ice-sheet (Rignot *et al* 2019) showed the ice-sheet has been actively interacting with the other climate systems on sub-centennial timescales (Nowicki *et al* 2016), emphasizing the need to investigate the impact of the ice-sheet on the earth system.

Recent studies have suggested that an increase in the meltwater flux can induce significant physical changes, such as the expansion of the sea-ice and subsurface warming in the SO (Bintanja *et al* 2013, 2015, Pauling *et al* 2016, 2017, Bronselaer *et al* 2018, Park and Latif 2019, Oh *et al* 2020). These changes were largely attributed to the suppressed deep convection in the SO, since the low density of meltwater inhibits the intrusion of warm circumpolar deep water into the surface. Meltwater-induced ocean stabilization also modulates various biogeochemical changes in the SO (Bronselaer *et al* 2020); for example, anomalous deoxygenation, acidification and nitrate decrease in the surface-to-subsurface water and increase in the deep water. The meltwater-driven reduced upwelling induces the variations by maintaining older, oxygen-poor, carbon-rich, and nitrate-poor water near the surface. However, the changes in iron concentration,

which generally is the most limiting nutrient for phytoplankton growth in the SO (Boyd *et al* 2007, Moore *et al* 2013, Laufkotter *et al* 2015) and resultant biomass changes associated with Antarctic meltwater-driven stratification, have not been addressed yet. Several works based on both observations and earth system models have only investigated the effects of the iron contained in the Antarctic meltwater, which can act to fertilize the SO (Death *et al* 2014, Laufkötter *et al* 2018, Person *et al* 2019).

Meanwhile, SO biogeochemical changes are noteworthy, considering the SO's role as a sink for anthropogenic CO_2 (Long *et al* 2021) and the role of the northward transport of nutrients in controlling low-latitude productivity (Sarmiento *et al* 2004, Laufkötter and Gruber 2018). Future projections in net-primary productivity in the SO exhibited considerable intermodel consistency in CMIP5 and CMIP6 under extreme warming scenarios (Bopp *et al* 2013, Laufkotter *et al* 2015, Kwiatkowski *et al* 2020). The decrease in the sea-ice cover in the SO in response to greenhouse warming may increase light availability for phytoplankton and therefore increase overall productivity (Doney 2006, Bopp *et al* 2013, Cabré *et al* 2015, Kwiatkowski *et al* 2020). However, these projections did not include the effects of Antarctic meltwater on marine nutrient cycling and resultant biomass changes.

Here, we perform a series of earth system model experiments to examine how the nutrients change and how they affect the chlorophyll concentration in the SO in response to Antarctic meltwater-induced ocean stabilization. In particular, we focus on changes in chlorophyll to investigate dynamical changes of phytoplankton biomass with variations in the limiting factors controlling biomass in the SO.

2. Data and methods

To examine the impacts of Antarctic meltwater forcing variations in SO chlorophyll, we performed idealized ensemble experiments with the Geophysical Fluid Dynamics Laboratory (GFDL) model CM2.1 (Delworth *et al* 2006) coupled with the marine ecosystem model Tracers of Phytoplankton with Allometric Zooplankton version 2 (TOPAZv2) (Dunne *et al* 2013). The version of GFDL-CM2.1-TOPAZv2 used here is the same as that used in (Lim *et al* 2018, 2019), and a detailed description of the model is available in the supplementary material.

Three different simulations were conducted. The first is a long-term control simulation (CTRL) over 2000 years applying a fixed atmospheric CO_2 concentration of 353 parts per million (ppm), corresponding to the 1990 level. The CTRL experiment in the present study was analyzed only for the last 1000 years to avoid long-term drift. The other two experiments are global warming simulations, with increasing atmospheric CO_2 concentration at a rate of 1% yr^{-1} until it doubled (706 ppm) from years 1–70 in the model, and held constant thereafter. The one (GW; global warming) simulation does not include Antarctic meltwater forcing, but the second (GWMW; GW plus Antarctic meltwater forcing) includes it. For each simulation, eight ensemble members were performed over 100 years. The individual ensemble members start from the different initial conditions taken from CTRL every 100 years, with the same model and boundary conditions. The meltwater forcing in GWMW was introduced at the surface and assumed to be a result of ice-sheet/shelf melting (figure S1(a) available online at stacks.iop.org/ERL/17/024022/mmedia). The total magnitude of the forcing is 0.2 Sv and constant in time, corresponding to the year 2050 meltwater estimates in historical and representative concentration pathways 8.5 scenario (DeConto and Pollard 2016). Most of the meltwater (64% of the total) is concentrated around West Antarctica, similar to recent observations of Antarctic glacial melting patterns (Shepherd *et al* 2018, Rignot *et al* 2019).

There are three phytoplankton groups (small, large and diazotrophs) in TOPAZv2. The zooplankton effects are represented implicitly and the grazing is based on (Dunne *et al* 2005). The nutrient limitation is determined by the minimum value among Fe, PO_4, and $NO_3 + NH_4$ limitation terms. The TOPAZv2 considers only two iron sources: atmospheric dust deposition based on a dust climatology (Fan *et al* 2006) and marginal sediment flux, parametrized as a function of the organic matter supply (Dunne *et al* 2013) (see supplementary for details). Because there is no iron in the meltwater in the present model experiments, the difference in the iron concentration changes between the GW and GWMW can be interpreted as a result of the meltwater-induced ocean stabilization. Note that all analyses were based on the December–February (DJF) period because the chlorophyll change between GW and GWMW was the largest in the DJF season in the SO (figure S3). To test the statistical significance of the ensemble mean difference and the regression coefficients, the bootstrap method (details in the supplementary) and student's t-test were used, respectively.

3. Results

To examine the impact of Antarctic meltwater forcing, we first analyzed the ensemble mean difference of surface-layer (upper 30 m average) chlorophyll concentration between the GWMW and GW experiments during the austral summer. As shown in figures 1(a) and (b), there is an increase in the surface chlorophyll concentrations in the regions more than 200 km from the Antarctic coastline in response to the meltwater forcing. Interestingly, however, the chlorophyll concentration significantly decreases in the marginal sea along the coastline. The

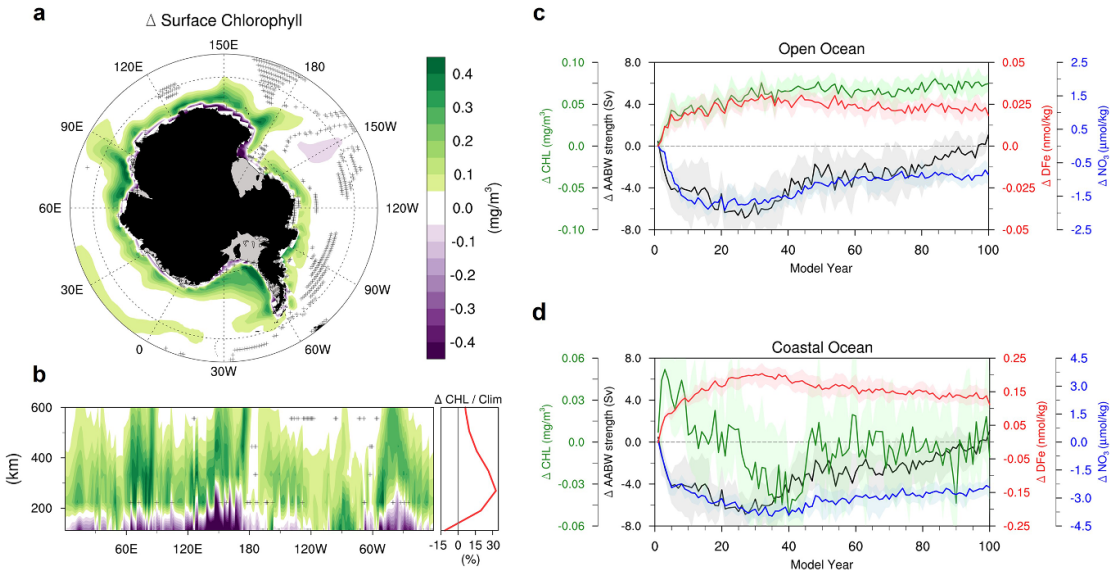

Figure 1. (a) Ensemble mean difference (GWMW − GW) of the surface (upper 30 m average) chlorophyll concentration averaged over the DJF season during the entire simulation period. (b) Same as in panel (a) but shows the results with longitude and distance from the continent. The rightmost red line is the percentage of the anomalies with respect to the climatology in CTRL (DJF-mean). Cross-shaped dots indicate where the differences are insignificant at the 99% confidence level using the bootstrap method. Time evolution of surface chlorophyll (CHL, green), dissolved iron (DFe, red), and nitrate (NO_3, blue) concentration averaged over the (c) open and (d) coastal oceans (defined in figure S1(b)) and the AABW strength (black) in the ensemble mean difference. Shading shows 99% uncertainty in the mean.

percentage of the changes in chlorophyll concentration, averaged across longitudes the same distance from the continent relative to the value in CTRL simulation, is in the rightmost red line in figure 1(b).

Figures 1(c) and (d) show the time evolution of the surface (upper 30 m average) chlorophyll (CHL), dissolved iron (DFe), and nitrate (NO_3) concentration anomalies averaged over the open and coastal oceans. The coastal ocean is defined as regions up to a 220 km line from the coastline and the open ocean is defined as regions from the northern edge of the coastal ocean to 60 °S (see figure S1(b)). The CHL anomalies in the open ocean are positive over the entire period (figure 1(c)). The positive anomalies in the open ocean gradually increase over the first 40 years and remain constant for the rest of the simulation. In the coastal ocean however, the CHL anomalies decrease over the first 40 years and then gradually recover (figure 1(d)). These evolutions of CHL seem to be related to NO_3 and DFe evolutions, which are influenced by vertical oceanic mixing. As a proxy for the vertical mixing in the SO, we adopted the Antarctic bottom water (AABW) strength (Zhang *et al* 2019). The AABW strength, black line in figures 1(c) and (d), is defined as the absolute value of the minimum in the global overturning stream function south of 60 °S (more commonly referred to as the strength of the lower overturning cell). In figures 1(c) and (d), the AABW strength in GWMW declines as compared to that in the GW simulation, indicating reduced deep convection in the SO (figure S2). Changes in this proxy can largely explain changes in NO_3 and DFe concentrations in both regions with positive and negative correlation coefficients (AABW strength versus NO_3 and DFe; based on interannual anomalies of the ensemble mean) as follows: $r_{\text{nitrate}} = 0.82^{**}$ and $r_{\text{iron}} = -0.40^{**}$ (for the open ocean) and $r_{\text{nitrate}} = 0.61^{**}$ and $r_{\text{iron}} = -0.62^{**}$ (for the coastal ocean). The ** mark indicates that the correlation coefficient is significant at the 99% confidence level. This suggests that a decline in the strength of deep convection leads to a reduction in NO_3 availability, but an increase in DFe.

The NO_3 concentration decreases in both regions, consistent with previous findings (Bronselaer *et al* 2020). However, the DFe concentration rather increases in both regions for the same reduction of oceanic deep convection. The increase in DFe covaries with an increase in CHL in the open ocean because of the iron limitation in the SO with a positive correlation coefficient (based on interannual anomalies of the ensemble mean) of 0.73^{**}. Accordingly, there is little correlation with the NO_3 concentration ($r = -0.03$). Conversely, the CHL concentration decreases in the coastal ocean despite the DFe increase. It appears that the CHL anomaly rather follows the NO_3 change ($r = 0.64^{**}$) but has a negative relationship with the DFe change ($r = -0.55^{**}$), suggesting that DFe is not the limiting nutrient in the coastal ocean. In the following two sections, we will focus on two contrary responses to the Antarctic meltwater forcing: (a) the NO_3 decrease and DFe increase and (b) the CHL increase in the open ocean and decrease in the coastal ocean.

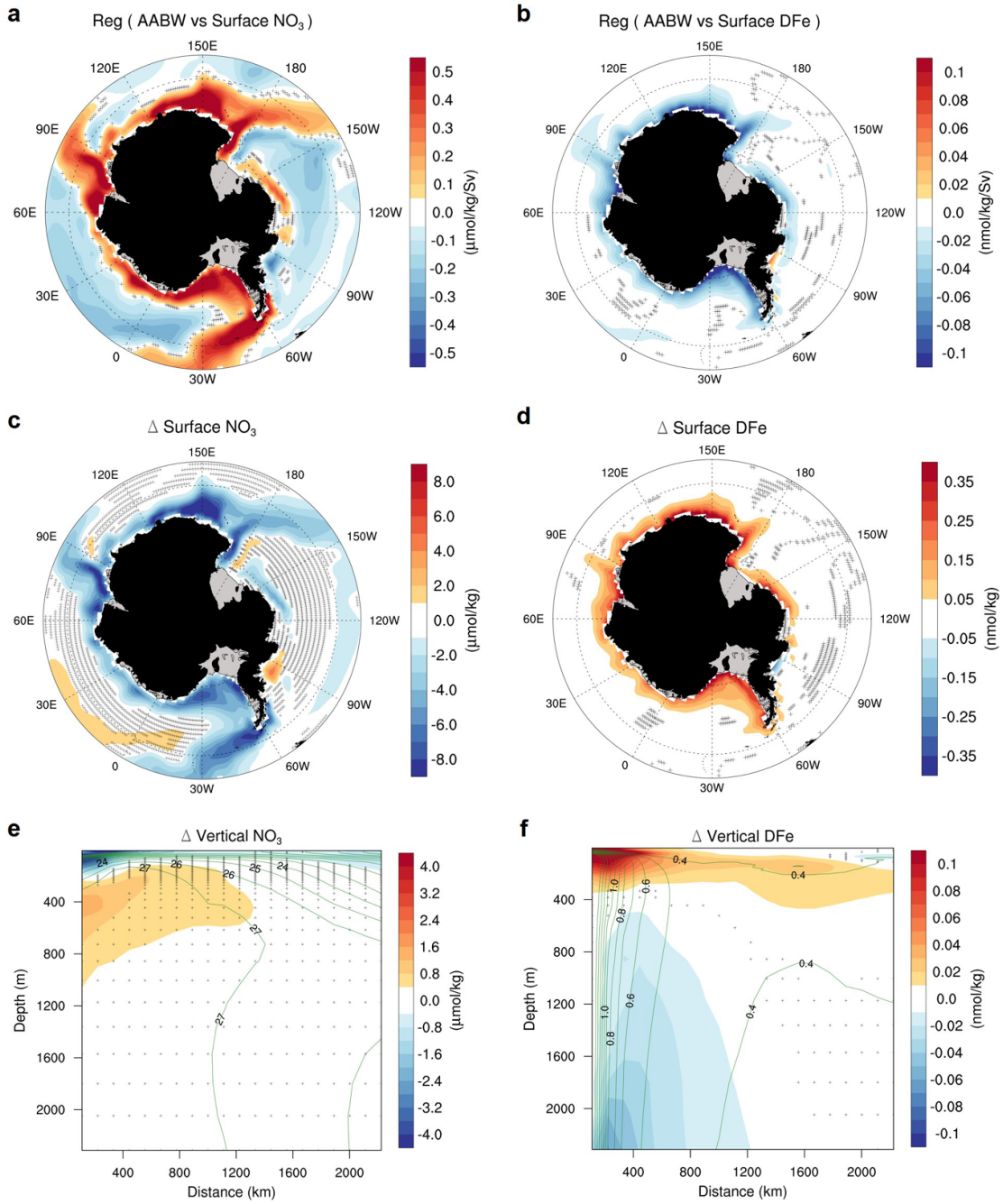

Figure 2. Regression coefficients of the (a) surface (upper 30 m average) NO_3 concentration and (b) the DFe concentration onto the AABW strength. Values are calculated in the DJF-mean in all experiments. The ensemble mean difference (GWMW − GW) of the (c) surface NO_3, (d) DFe, (e) vertical NO_3, and (f) DFe concentrations in the DJF-mean during the 21–40 simulation period. The green contours in panels (e) and (f) indicate the DJF-mean climatology (CTRL) of NO_3 (1.0 μmol kg^{-1} interval) and DFe (0.1 nmol kg^{-1} interval) respectively. Panels (e) and (f) are averaged based on the same distance from the Antarctic coastline. Cross-shaped dots indicate where the differences are insignificant at the 99% confidence level by using student's t-test in panels (a), (b) and the bootstrap method in panels (c)–(f).

3.1. Contrary responses in NO_3 and DFe concentrations

Figures 2(a) and (b) show the linear regression coefficient of the surface NO_3 and DFe concentrations against the AABW strength by using all three simulations (CTRL, GW, and GWMW) data. The AABW strength shows an overall positive and negative relationship with NO_3 and DFe respectively. The surface NO_3 and DFe changes for the glacial meltwater are highly consistent with these results, as shown in figures 2(c) and (d). To check this further, we investigated the vertical changes in NO_3 and DFe for the Antarctic meltwater forcing. Indeed, as shown in figures 2(e) and (f), NO_3 decreases in the upper ocean but increases in the abyssal ocean while the DFe shows the opposite response.

These contrary responses in the NO_3 and DFe in the SO may depend on the differing sources, which

determine the vertical distributions of the NO_3 and DFe. A decrease in the surface NO_3 can be attributed to a weakened nutrient supply to the mixed layer due to the meltwater-induced freshening, which inhibits the upwelling of nitrate-rich deep water to the surface-to-subsurface water (Bronselaer *et al* 2020). Also, the surface NO_3 decrease is partly due to the enhanced uptake by the phytoplankton. Climatological values of the NO_3 and DFe concentrations in the CTRL are presented via the contours in figures 2(e) and (f). In the overall SO, the climatological NO_3 concentration is relatively high in the deep ocean and the open ocean. Note that TOPAZv2 includes external atmospheric inputs and river nitrogen discharged into the surface (Dunne *et al* 2013) (see supplementary), so that the enhanced stability may also play a role in enhancing the concentration of certain sources of nitrogen in the surface ocean. But given that NO_3 decreases, this cannot be the reason and instead suggests that this decrease is mainly driven by a decline in vertical supply from the nitrate-rich deep water.

In contrast to NO_3, the climatological DFe in the CTRL is highly concentrated along the Antarctic coastline, with a maximum value near a depth of 200 m. The DFe concentration gradually decreases with depth in contrast to the NO_3 concentration. Marginal sediment sources discharged into the upper ocean on the shelf are responsible for this spatial and vertical distribution of the DFe. In response to the weakened deep convection due to the meltwater-induced freshening, the iron supply from the upper ocean on the shelf to the deep ocean decreases. Therefore, iron from marginal sediments is trapped in the upper ocean, resulting in a DFe increase in the surface (figures 2(d)–(f)). In addition, iron from the air deposition goes through the same process, contributing to the surface DFe increase. To sum up, given the same meltwater-induced stabilization, NO_3 and DFe show contrasting responses between the coastal and open ocean, depending on the depth of their main sources.

3.2. Regime shift in the marginal sea along the Antarctic coastline

To understand the contrasting responses of surface CHL concentration between the coastal and open ocean, figures 3(a) and (b) relate the distribution of surface CHL and DFe anomalies relative to the long-term mean in the CTRL. In the open ocean, the CHL anomaly has a significant positive relationship with the DFe anomaly in all experiments (figure 3(a)). This suggests that the iron limitation on the CHL growth is being maintained in the open ocean in both GW and GWMW. However, in the GWMW simulation, the positive relationship between DFe and CHL tends to be weakened at high DFe levels.

In the coastal ocean, the CTRL and GW simulations also show a positive linear relationship between the CHL and DFe concentrations, suggesting that the CHL increases as DFe increases (figure 3(b)). Note that the DFe concentration anomaly does not exceed 0.04 nmol kg^{-1} in the CTRL and GW simulations. In the GWMW simulation, however, the relationship is quite different from that in the open ocean. For a DFe concentration of 0.04–0.1 nmol kg^{-1}, which is much greater than the concentration in the open ocean, the CHL anomalies are positive but much smaller than those in the open ocean and a linear relationship is not seen. This suggests that the DFe in this range does not drive an additional increase in the CHL, indicating that the iron limitation regime is no longer in effect. Interestingly, when the DFe concentration is greater than 0.1 nmol kg^{-1}, the CHL responds negatively to increases in the DFe. This nonlinear CHL response cannot be well understood by only considering changes in DFe.

To understand this nonlinear CHL response to DFe in the coastal ocean, we divided the results into three subsets depending on the DFe concentration anomaly in figures 3(a) and (b) and computed the regression coefficients of the CHL concentration against DFe and NO_3 in each subset (figures 3(c) and (d)). When the DFe concentration is relatively small (the left two columns in figures 3(c) and (d)), the DFe is strongly responsible for the growth of the CHL in the overall SO, while the role of the NO_3 is relatively weak. However, as the DFe concentration increases, as in the right column in figures 3(c) and (d), the importance of the DFe becomes weak and even shows a negative relationship in the coastal ocean. Concurrently, the role of the NO_3 in CHL increase becomes important in the coastal ocean. This means that the surface CHL more depends on the NO_3 than on the DFe in the coastal ocean at high DFe levels, implying that the limiting nutrient for CHL has shifted from the iron to the nitrate. From these results, the decrease in deep convection results in a decrease in the NO_3 concentrations, hence, the CHL concentration decreases in the coastal ocean as shown in figures 1(a) and (b). Note that the DFe and NO_3 gradually recover in the coastal ocean as the AABW strength recovers after the first 40 years (figure 1(d)). At the same time, the CHL concentration also recovers, implying the limiting nutrient in the coastal ocean slowly changes from nitrate to iron again.

To further support this argument, figure 4 shows the distribution of CHL concentration against the DFe and NO_3 concentrations by averaging the values at all grid points and in all months from all ensembles and experiments in the open and coastal oceans respectively. As shown in figures 4(a) and (b), the CHL sharply increases as the DFe increases when the ratio of DFe to NO_3 is relatively large (a strong x-direction gradient, iron-limited regime). However, if the ratio of DFe to NO_3 becomes relatively small, nitrate plays an important role in the growth of

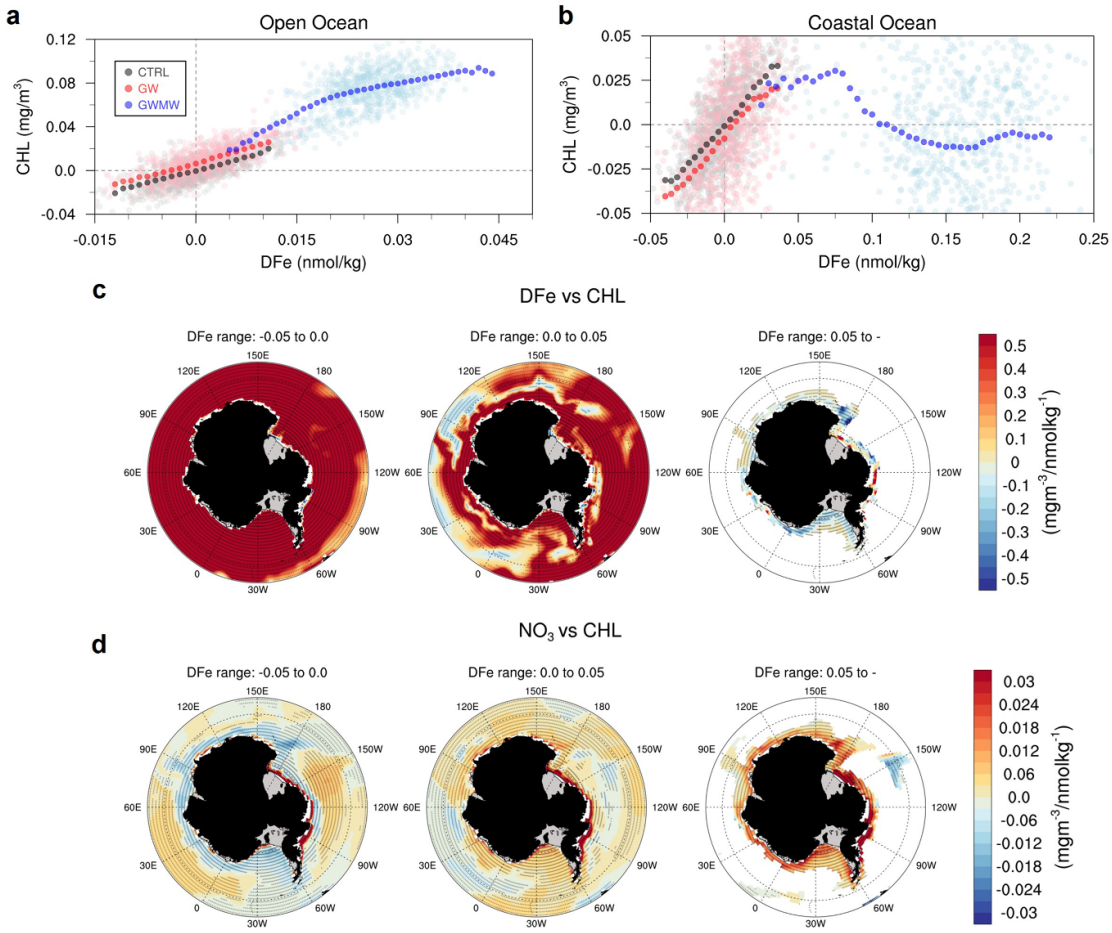

Figure 3. Distributions of the DFe and surface CHL concentration anomalies (DJF-mean) in CTRL (grey), GW (light-red), and GWMW (light-blue) relative to CTRL averaged over the (a) open and (b) coastal oceans (defined in figure S1(b)) in each ensemble and year during the entire simulation. Thick dots indicate the average in every given (a) 0.006, (b) 0.02 (CTRL, GW) and (a) 0.01, (b) 0.05 (GWMW) bin of the DFe concentration (nmol/kg) with a (a) 0.0012, (b) 0.004 (CTRL, GW) and (a) 0.001, (b) 0.005 (GWMW) step moving average. Regression coefficients of the CHL concentration onto the (c) DFe and (d) NO_3 concentrations given for each DFe range. Values are calculated in the DJF-mean cases in all experiments. Dots indicate where the responses are significant at the 99% confidence level by using the student's t-test.

CHL (a strong *y*-direction gradient, nitrate-limited regime).

In the open ocean, the mean positions of the CTRL and GW are located in the iron limitation regime where the *x*-direction gradient is strong. In addition, in the GWMW, even though the mean position moves slightly to the right and south (NO_3 decrease and DFe increase), it is still in the iron-limited regime, such that the CHL increases as the DFe increases in the open ocean (figures 1(a) and (b)). In the coastal ocean, the mean positions of the CTRL and GW are located in the iron limitation regime, while that of the GWMW is in the nitrate-limited regime where the *y*-direction gradient is strong. This is consistent with the negative response of the CHL concentration as the NO_3 concentration decreases in the coastal ocean (figures 1(a) and (b)).

The differences in magnitude in the climatological nutrients between the open and coastal oceans are important for the regime shift. As shown in the mean positions in figure 4, the higher NO_3 and lower DFe concentrations in the open ocean, compared to in the coastal ocean, are unfavorable to a regime shift due to glacial meltwater in the open ocean. That is, in the open ocean, a larger DFe increase and NO_3 decrease (meltwater-induced nutrient changes) are required to shift the area from an iron-limited to a NO_3-limited regime. Compared with the open ocean, it is easier to shift the nutrient limitation regime in the coastal ocean (a relatively smaller anomaly is required). Even the magnitude of the nutrient changes in response to the meltwater forcing is much smaller in the open ocean than in the coastal ocean. This means that the nutrient changes in the open ocean are not sufficient to shift the nutrient regime. Therefore, Antarctic glacial meltwater can induce a contrary CHL concentration response in the open ocean and the coastal ocean.

4. Summary and discussion

Here, we examined the Antarctic glacial meltwater impacts (ocean stabilization) on the nutrients and

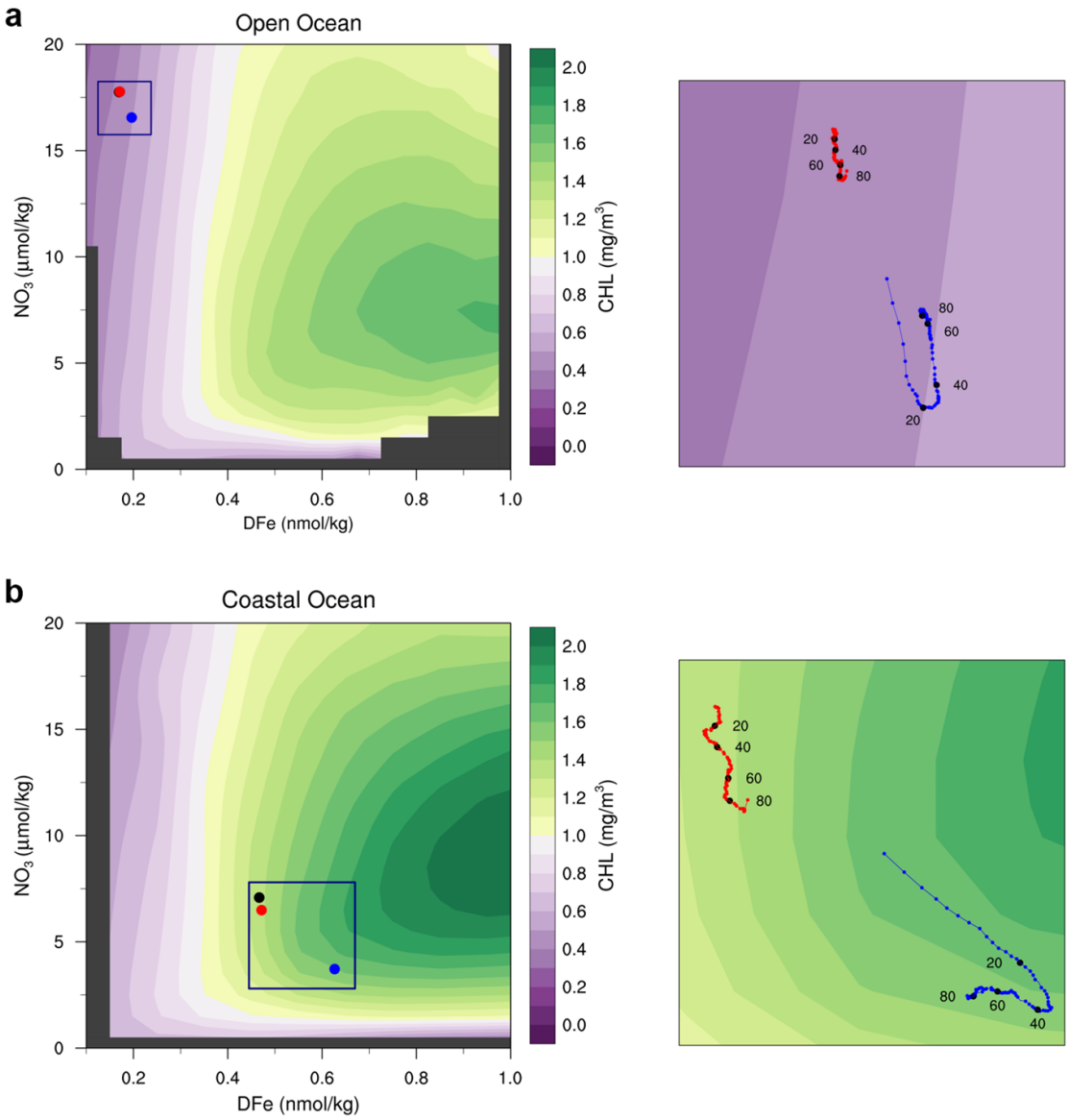

Figure 4. Surface CHL concentration responses to the surface DFe and NO_3 concentrations in all experiments (CTRL, GW, and GWMW), ensembles, months (DJF), and grid points in the (a) open and (b) coastal oceans during the entire simulation. At a resolution of 1°, there are 3197 grid points for the open ocean and 883 grid points for the coastal ocean (defined in figure S1(b)), corresponding to a total of 24 936 600 and 6887 400 cases respectively. Dots indicate the average in all ensembles, months, time-steps, and grid points in each experiment (CTRL: black, GW: red, and GWMW: blue). The small dots in the right panels indicate the time evolution in GW (red) and GWMW (blue) with an 11 year moving average.

subsequent CHL changes using a series of earth system model simulations. Because there is no iron contained in Antarctic meltwater in the model in the present study, the change in iron is only due to ocean stabilization. In response to the glacial meltwater forcing, a NO_3 decrease (increase) in the upper (deep) ocean was shown in the present study, consistent with previous findings (Bronselaer *et al* 2020). However, changes in the DFe had opposite responses to the changes in the NO_3. The contrary responses in the NO_3 and DFe to the meltwater forcing depended on the depth of the main source being from the upper or deep ocean. Accordingly, the surface CHL increased in the open ocean as the DFe increased. However, in the narrow coastal regions, the CHL decreased in response to the meltwater forcing, which was attributed to a dramatic regime shift in the coastal regions from the iron-limited to the nitrate-limited conditions.

Direct iron supply from Antarctic glacial meltwater, a largely overlooked source in most marine ecosystem models (Tagliabue *et al* 2016), has been investigated in many recent studies (Death *et al* 2014, Raiswell *et al* 2016, Laufkötter *et al* 2018, Person *et al* 2019). Antarctic glacial meltwater is introduced into the upper ocean such that the resultant direct iron input to the SO is concentrated on the upper ocean. This glacial iron supply can contribute to iron trapping in the upper ocean due to the meltwater-induced enhanced stratification, via the same process as the

marginal sediment and atmospheric dust iron sources in this study. Considering the glacial iron sources, the responses in this study would be amplified. For example, it could induce more surface iron increase and the expansion of nutrient regime shift region.

In this study, we mostly focused on the DJF season because the CHL response to the addition of meltwater is strongest and it explains most of the total CHL changes (figure S3). In addition, we paid attention to the nutrient limitation because the light limitation does not play a dominant role in most SO during the summer season, due to enough light and nutrients depleted by the spring phytoplankton (Lim *et al* 2019). Indeed, there are negative relationships in DJF between incoming shortwave radiation and surface CHL not only in the GW but also in the GWMW (figures S4(a) and (b)), implying a minor role of the light limitation compared with the nutrient limitation in the meltwater-induced CHL changes in this study. On the other hand, the relationships become positive around Antarctica in the September-November (SON) season (austral spring) (figures S4(c) and (d)), implying a dominant role of the light limitation because of the sufficient nutrients in the spring due to the small phytoplankton biomass in the winter season (Lim *et al* 2019). The CHL changes in the SON season are relatively weak and showed a somewhat different spatial distribution from the DJF case (figure S3), which might be associated with light limitation changes in response to the meltwater-induced sea ice increase.

The present study concentrated on the CHL responses, which can induce biogeophysical feedback that affects radiant heating by the reduction of surface albedo and shortwave penetration (Frouin 2002, Park *et al* 2015, Lim *et al* 2019) and can be used for global fish catch prediction (Friedland *et al* 2012, Park *et al* 2019). In addition, the changes of vertically integrated CHL concentration (figure S5) in the euphotic zone (top 100 m) as a proxy of primary productivity, exhibit an overall increase around Antarctica, indirectly showing the enhanced carbon uptake. Indeed, the dissolved inorganic carbon concentration decreases in the surface layer (figure S6), which possibly implies enhanced carbon uptake by the phytoplankton and consequent downward carbon export increase, thus this leads to the increase in pH and oxygen concentration in the surface (figure S6). However, the meltwater-induced stratification and resultant surface cooling and subsurface warming also can contribute to these pH and oxygen changes. For example, the pH and oxygen concentration decrease in the deep ocean because more organic carbon can be remineralized due to the isolation of carbon-rich deep water from the surface by the stratification. The surface cooling and subsurface warming lead to the increase and decrease of the oxygen concentration in the surface layer and deep ocean by the solubility changes respectively. Therefore, a comprehensive understanding of how the physical and biogeochemical factors driven by the Antarctic meltwater can interact with each other is necessary for the meltwater-induced carbon uptake and export changes. Moreover, each functional type of phytoplankton has a different degree of limitation strength for each nutrient, so that the phytoplankton community composition can also change in the SO in response to the Antarctic meltwater. However, a comprehensive analysis of the carbon uptake, export, and phytoplankton community changes in the SO due to the glacial meltwater was not addressed here in detail. These points, which have importance to the global carbon cycle are meaningful and should be addressed in further study.

Our results were based on a single earth system model study, so that they could be model dependent. As demonstrated in (Tagliabue *et al* 2016), TOPAZv2 overestimates DFe in the surface ocean and underestimates it in the ocean interior, which might be associated with the absence of hydrothermal sources (Tagliabue *et al* 2010) and large marginal sediment sources or an iron-binding ligand concentration. Also, the surface NO_3 concentration in the coastal region around Antarctica is underestimated in TOPAZv2 (Séférian *et al* 2020). These characteristics of TOPAZv2 might result in sufficient DFe and NO_3 deficit in the surface ocean by the meltwater forcing and consequent nutrient regime shift from the iron-limited to nitrate-limited in the coastal region in this study. There are severe uncertainties in the parameterizations of all aspects of the iron cycle, including the magnitude and variability of the diverse iron sources, solubility, and chemistry in the ocean (Boyd *et al* 2012, Tagliabue *et al* 2016). Thus, whether the present results are definitive is beyond the scope of a single model study. Analyses from multi-model intercomparisons and advanced coupled climate-land ice models with various nutrient sources are necessary to test the robustness of our findings.

Data availability statement

Processed model data will be available through this link https://doi.org/10.6084/m9.figshare.14183072

The data that support the findings of this study are available upon reasonable request from the authors.

Acknowledgments

This work was sponsored by a research grant from the Korean Ministry of Oceans and Fisheries (KIMST20190361 and PM20020), and the National Research Foundation of Korea (NRF-2021M3I6A1086808).

ORCID iDs

Ji-Hoon Oh https://orcid.org/0000-0001-8484-8997
Jong-Seong Kug https://orcid.org/0000-0003-2251-2579

References

Bintanja R, Van Oldenborgh G J, Drijfhout S S, Wouters B and Katsman C A 2013 Important role for ocean warming and increased ice-shelf melt in Antarctic sea-ice expansion *Nat. Geosci.* **6** 376–9
Bintanja R, Van Oldenborgh G J and Katsman C A 2015 The effect of increased fresh water from Antarctic ice shelves on future trends in Antarctic sea ice *Ann. Glaciol.* **56** 120–6
Bopp L *et al* 2013 Multiple stressors of ocean ecosystems in the 21st century: projections with CMIP5 models *Biogeosciences* **10** 6225–45
Boyd P W *et al* 2007 Mesoscale iron enrichment experiments 1993–2005: synthesis and future directions *Science* **315** 612–7
Boyd P W, Arrigo K R, Strzepek R and van Dijken G L 2012 Mapping phytoplankton iron utilization: insights into Southern Ocean supply mechanisms *J. Geophys. Res. Ocean.* **117** C06009
Bronselaer B, Russell J L, Winton M, Williams N L, Key R M, Dunne J P, Feely R A, Johnson K S and Sarmiento J L 2020 Importance of wind and meltwater for observed chemical and physical changes in the Southern Ocean *Nat. Geosci.* **13** 35–42
Bronselaer B, Winton M, Griffies S M, Hurlin W J, Rodgers K B, Sergienko O V, Stouffer R J and Russell J L 2018 Change in future climate due to Antarctic meltwater *Nature* **564** 53–58
Cabré A, Marinov I and Leung S 2015 Consistent global responses of marine ecosystems to future climate change across the IPCC AR5 earth system models *Clim. Dyn.* **45** 1253–80
Death R, Wadham J L, Monteiro F, Le Brocq A M, Tranter M, Ridgwell A, Dutkiewicz S and Raiswell R 2014 Antarctic ice sheet fertilises the Southern Ocean *Biogeosciences* **11** 2635–43
DeConto R M and Pollard D 2016 Contribution of Antarctica to past and future sea-level rise *Nature* **531** 591–7
Delworth T L *et al* 2006 GFDL's CM2 global coupled climate models. Part I: formulation and simulation characteristics *J. Clim.* **19** 643–74
Doney S C 2006 Plankton in a warmer world *Nature* **444** 695–6
Dunne J P *et al* 2013 GFDL's ESM2 global coupled climate-carbon earth system models. Part II: carbon system formulation and baseline simulation characteristics *J. Clim.* **26** 2247–67
Dunne J P, Armstrong R A, Gnanadesikan A and Sarmiento J L 2005 Empirical and mechanistic models for the particle export ratio *Glob. Biogeochem. Cycles* **19** GB4026
Eyring V, Bony S, Meehl G A, Senior C A, Stevens B, Stouffer R J and Taylor K E 2016 Overview of the coupled model intercomparison project phase 6 (CMIP6) experimental design and organization *Geosci. Model Dev.* **9** 1937–58
Fan S M, Moxim W J and Levy H 2006 Aeolian input of bioavailable iron to the ocean *Geophys. Res. Lett.* **33** L07602
Fogwill C J, Phipps S J, Turney C S M and Golledge N R 2015 Sensitivity of the Southern Ocean to enhanced regional Antarctic ice sheet meltwater input *Earth's Future* **3** 317–29
Friedland K D, Stock C, Drinkwater K F, Link J S, Leaf R T, Shank B V, Rose J M, Pilskaln C H and Fogarty M J 2012 Pathways between primary production and fisheries yields of large marine ecosystems *PLoS One* **7** e28945
Frouin R 2002 Influence of phytoplankton on the global radiation budget *J. Geophys. Res.* **107** 4377
Hansen J *et al* 2016 Ice melt, sea level rise and superstorms: evidence from paleoclimate data, climate modeling, and modern observations that 2 °c global warming could be dangerous *Atmos. Chem. Phys.* **16** 3761–812
Konrad H, Shepherd A, Gilbert L, Hogg A E, McMillan M, Muir A and Slater T 2018 Net retreat of Antarctic glacier grounding lines *Nat. Geosci.* **11** 258–62
Kwiatkowski L *et al* 2020 Twenty-first century ocean warming, acidification, deoxygenation, and upper ocean nutrient decline from CMIP6 model projections *Biogeosci. Discuss.* **17** 3439–70
Laufkotter C *et al* 2015 Drivers and uncertainties of future global marine primary production in marine ecosystem models *Biogeosciences* **12** 6955–84
Laufkötter C and Gruber N 2018 Will marine productivity wane? *Science* **359** 1103–4
Laufkötter C, Stern A A, John J G, Stock C A and Dunne J P 2018 Glacial iron sources stimulate the southern ocean carbon cycle *Geophys. Res. Lett.* **45** 13377–85
Lim H G, Kug J S and Park J Y 2019 Biogeophysical feedback of phytoplankton on the Arctic climate. Part I: impact of nonlinear rectification of interactive chlorophyll variability in the present-day climate *Clim. Dyn.* **52** 5383–96
Lim H G, Park J Y and Kug J S 2018 Impact of chlorophyll bias on the tropical Pacific mean climate in an earth system model *Clim. Dyn.* **51** 2681–94
Long M C *et al* 2021 Strong Southern Ocean carbon uptake evident in airborne observations *Science* **374** 1275–1280
Moore C M *et al* 2013 Processes and patterns of oceanic nutrient limitation *Nat. Geosci.* **6** 701–10
Nowicki S M J, Payne A, Larour E, Seroussi H, Goelzer H, Lipscomb W, Gregory J, Abe-Ouchi A and Shepherd A 2016 Ice sheet model intercomparison project (ISMIP6) contribution to CMIP6 *Geosci. Model Dev.* **9** 4521–45
Oh J, Park W, Lim H, Noh K M, Jin E K and Kug J 2020 Impact of Antarctic meltwater forcing on East Asian climate under greenhouse warming *Geophys. Res. Lett.* **47** e2020GL089951
Paolo F S, Fricker H A and Padman L 2015 Volume loss from Antarctic ice shelves is accelerating *Science* **348** 327–31
Park J Y, Kug J S, Bader J, Rolph R and Kwon M 2015 Amplified Arctic warming by phytoplankton under greenhouse warming *Proc. Natl Acad. Sci. USA* **112** 5921–6
Park J-Y, Stock C A, Dunne J P, Yang X and Rosati A 2019 Seasonal to multiannual marine ecosystem prediction with a global Earth system model *Science* **365** 284–8
Park W and Latif M 2019 Ensemble global warming simulations with idealized Antarctic meltwater input *Clim. Dyn.* **52** 3223–39
Pauling A G, Bitz C M, Smith I J and Langhorne P J 2016 The response of the Southern Ocean and Antarctic sea ice to freshwater from ice shelves in an earth system model *J. Clim.* **29** 1655–72
Pauling A G, Smith I J, Langhorne P J and Bitz C M 2017 Time-dependent freshwater input from ice shelves: impacts on Antarctic sea ice and the Southern Ocean in an earth system model *Geophys. Res. Lett.* **44** 10454–61
Person R, Aumont O, Madec G, Vancoppenolle M, Bopp L and Merino N 2019 Sensitivity of ocean biogeochemistry to the iron supply from the Antarctic ice sheet explored with a biogeochemical model *Biogeosciences* **16** 3583–603
Raiswell R *et al* 2016 Potentially bioavailable iron delivery by iceberg-hosted sediments and atmospheric dust to the polar oceans *Biogeosciences* **13** 3887–900
Rignot E, Mouginot J, Scheuchl B, Van Den Broeke M, Van Wessem M J and Morlighem M 2019 Four decades of Antarctic ice sheet mass balance from 1979–2017 *Proc. Natl Acad. Sci. USA* **116** 1095–103
Sarmiento J L, Gruber N, Brzezinski M A and Dunne J P 2004 High-latitude controls of thermocline nutrients and low latitude biological productivity *Nature* **427** 56–60

Séférian R et al 2020 Tracking improvement in simulated marine biogeochemistry between CMIP5 and CMIP6 *Curr. Clim. Change Rep.* **6** 95–119

Shepherd A, Ivins E, Rignot E, Smith B, Van Den Broeke M and Velicogna I 2018 Mass balance of the Antarctic ice sheet from 1992 to 2017 *Nature* **558** 219–22

Tagliabue A et al 2010 Hydrothermal contribution to the oceanic dissolved iron inventory *Nat. Geosci.* **3** 252–6

Tagliabue A et al 2016 How well do global ocean biogeochemistry models simulate dissolved iron distributions? *Glob. Biogeochem. Cycles* **30** 149–74

Taylor K E, Stouffer R J and Meehl G A 2012 An overview of CMIP5 and the experiment design *Bull. Am. Meteorol. Soc.* **93** 485–98

Wouters B, Martin-Español A, Helm V, Flament T, Van Wessem J M, Ligtenberg S R M, Van Den Broeke M R and Bamber J L 2015 Dynamic thinning of glaciers on the Southern Antarctic Peninsula *Science* **348** 899–903

Zhang L, Delworth T L, Cooke W and Yang X 2019 Natural variability of Southern Ocean convection as a driver of observed climate trends *Nat. Clim. Change* **9** 59–65